Computational and Experimental Study of the Cyclic Voltammetry Response of Partially Blocked Electrodes. Part 1. Nonoverlapping, Uniformly Distributed Blocking Systems

Benjamin A. Brookes,[†] Trevor J. Davies,[†] Adrian C. Fisher,[‡] Russell G. Evans,[†] Shelley J. Wilkins,[†] Kamran Yunus,[‡] Jay D. Wadhawan,[†] and Richard G. Compton*,[†]

Physical and Theoretical Chemistry Laboratory, Oxford University, South Parks Road, Oxford OX1 3QZ, United Kingdom, and Department of Chemistry, University of Bath, Claverton Down, Bath BA2 7AY, United Kingdom

Received: August 6, 2002; In Final Form: November 18, 2002

The cyclic voltammetry response of partially blocked electrodes is modeled using finite difference simulations and a method presented for determining currents at electrode surfaces which have a well-defined geometric blocking pattern. Peak current and peak separation data are presented for six decades of scan rates, blocking coverage values between 0.1 and 0.9 and between the limits of reversible and irreversible electrochemistry. The validity of the simulation approach employed is verified by data obtained experimentally from purpose-built partially blocked gold film electrodes, with either a cubic or hexagonal geometric array of electroinactive disks uniformly distributed on the electrode surface. Comparison of theory with experiment suggests that the modeling of hexagonally distributed blocking systems is superior to that of the cubically arranged ones.

1. Introduction

Electrochemistry at partially blocked electrodes (PBEs) presents an intriguing problem because the surface blocking of the electrode modifies the absolute and relative rates of diffusive and kinetic flux to the electrode surface.[1−20] Not only can these changes lead to inaccurate electrochemical interpretation but, in some circumstances, the blocked electrode may be mistaken for an unblocked one with the wrong mechanism.[1] Significant research has therefore been undertaken in order to quantify the electrochemistry at PBEs, with the main aim of producing a reliable method for interrogating the characteristics of the surface blocking with existing electrochemical techniques.

Since some of the earliest studies carried out by Landsberg,[2−8] results have been published for stationary and rotating disk PBEs with a particular emphasis on impedance techniques.[1−20] Most of the analytical theory accompanying these studies has been derived using underlying simplifications in order to reduce the complexity of the problem. The most unsatisfactory simplifications are highlighted[13,16] as (1) mass transport being formulated under steady-state conditions, (2) the implementation of a Nernst diffusion layer in stationary or rotating conditions, and (3) the omission of radial or axial convection terms. To a large degree, these are circumvented in analytical work by Matsuda[13−15] at stationary partially blocked electrodes, and results were presented for Faradaic impedance, chronoamperometry, chrono-potentiometry, and potential sweep voltammetry. Nevertheless, significant assumptions are introduced in this modeling in order to find a tractable solution. The inaccuracy of such results has been highlighted by data gathered from the numerical solution of the diffusion partial differential equations (PDE), a process

which is becoming increasingly favorable with recent advances in computers.[17,18,20] Extensive as the literature is, Amatore[16] has pointed out that the applicability of previous work has been limited to PBEs with macroscopic inhomogeneity, and so all electrochemistry must be considered diffusion limited. Amatore's one-dimensional formulation[16] of the model generates results and allows a method for surface characterization (where electrochemistry is not necessarily reversible) from cyclic voltammogram characteristics.

Many authors have performed experimental studies in order to validate theoretically generated results.[13−15] These employ model electrodes fabricated by several methods, including the use of photoresist layers,[13] laser ablation of metal surfaces,[10] and controlled sintering of metal powders followed by application of Araldite.[10] Where possible, the authors tried to maintain a regular geometry of blocking units in the model PBEs, for example cubic or hexagonal packing. To the authors' knowledge, the dependence of the electrode current on the electrode surface blocking geometry has not been investigated in an experimental context in any depth. This would seem reasonable given that many intrinsically inhomogeneous surfaces that might be experimentally studied would not replicate the geometric regularity of the model electrodes and the theory that accompanies it. Significant extensions of both theory and experimental models are required if the research is to be extended to incorporate such partially blocked electrodes.

The aim of this work is to, via a simulation approach, find a general method for characterizing the transient responses of PBEs where both the reversibility of the reaction and the diffusion layer length have a significant effect on the current. In this paper, the effects of blocking geometry on the cyclic voltammetric response are investigated using model gold film partially blocked electrodes in which disk shaped blocks are arranged in a cubic or hexagonally packed geometry. In subsequent work,[21] we will consider the effects of having a

---
* To whom correspondence should be addressed. E-mail: richard.compton@chemistry.oxford.ac.uk. Phone: +44 (0) 1865 275 413. Fax: +44 (0) 1865 275 410.
† Oxford University.
‡ University of Bath.

Study of Partially Blocked Electrodes. Part 1

J. Phys. Chem. B, Vol. 107, No. 7, 2003 **1617**

randomly dispersed "block" geometry and show how the simulations developed in this paper can be applied to study experimentally observed results.

2. Theory

We assume that the blocked surface is comprised of inert disks which contact the electrode surface through a circular base of surface radius, R_b. The diffusion around any block is symmetric in the radial direction and at a distance corresponding to half the mean center-to-center separation with the neighboring blocks, R_0. We therefore consider the partially covered electrode surface as an ensemble of independently interacting cylindrical units[22] (or *diffusion domains*) of radius R_0 through which no diffusional flux passes. Each diffusional domain is bounded at the bottom by the electrode surface which is centrally blocked by a circular disk of radius R_b. It should be noted that we have not specified that all diffusion domains need to be of the same size, and in fact, by considering the electrode surface to be comprised of diffusion domains of differing radial size, it may be possible to approximate the effect of the distribution of R_0 values that are experimentally observed. However, all of the experimental systems considered in this paper have constant R_0 values.

The coverage of each diffusion domain, θ, is given by the ratio of areas of the block and the surface:

$$\theta = \frac{\pi R_b^2}{\pi R_0^2} = \left(\frac{R_b}{R_0}\right)^2 \tag{1}$$

The above equation refers to coverage on a microscopic scale. The macroscopic or global coverage, Θ, is given by

$$\Theta = \frac{N_{block}\pi R_b^2}{A_{elec}} \tag{2}$$

where N_{block} is the number of inert disks/blocks on the electrode surface. In each of the experimental systems explored in this paper, the values of R_0 and R_b are constant. Under these conditions, the microscopic coverage, θ, is equal to the global coverage, Θ, because $A_{elec} = N_{block}\pi R_0^2$.

2.1. Mass Transport Equations. We consider a simple redox couple at the electrode surface which possesses Butler–Volmer kinetics
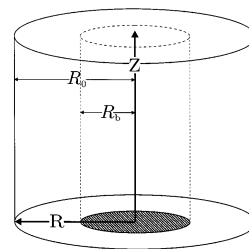
$$A \underset{k_b}{\overset{k_f}{\rightleftharpoons}} B + e^-$$
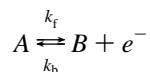
where $k_f = k° \exp[-\alpha nF/RT(E(t) - E°')]$ and $k_b = k° \exp[(1 - \alpha)nF/RT(E(t) - E°')]$. In the cylindrical polar coordinate system, the transport of both species A and B is described by the following linear partial differential equations

$$\frac{1}{D_a}\frac{\partial a}{\partial t} = \left\{\frac{\partial^2}{\partial Z^2} + \frac{\partial^2}{\partial R^2} + \frac{1}{R}\frac{\partial}{\partial R}\right\}a \tag{3}$$

$$\frac{1}{D_b}\frac{\partial a}{\partial t} = \left\{\frac{\partial^2}{\partial Z^2} + \frac{\partial^2}{\partial R^2} + \frac{1}{R}\frac{\partial}{\partial R}\right\}b \tag{4}$$

in which $a = [A]/[A]_{bulk}$, $b = [B]/[A]_{bulk}$, and D_a and D_b are the diffusion coefficients of the respective species. Figure 1

Figure 1. Illustration of the cylindrical polar coordinate system used to model the blocked electrode surface.

illustrates the geometry of the problem. The boundary conditions applicable to the above are

electrode	$Z = 0$	$R_b \leq R \leq R_0$	$D_a\frac{\partial a}{\partial Z} = -k_f a_0 + k_b b_0 = -D_b\frac{\partial b}{\partial Z}$
block	$Z = 0$	$0 \leq R < R_b$	$D_a\frac{\partial a}{\partial Z} = 0$ $D_b\frac{\partial b}{\partial Z} = 0$
axis of symmetry	$0 < Z < \infty$	$R = 0$	$\frac{\partial a}{\partial R} = 0$ $\frac{\partial b}{\partial R} = 0$
cylinder edge	$0 < Z < \infty$	$R = R_0$	$\frac{\partial a}{\partial R} = 0$ $\frac{\partial b}{\partial R} = 0$
diffusion layer	$Z \to \infty$	$0 \leq R \leq R_0$	$\frac{\partial a}{\partial Z} = 0$ $\frac{\partial b}{\partial Z} = 0$

where a_0 and b_0 are the normalized concentrations of A and B at the electrode surface, and the height of the blocking disk is neglected (but nevertheless assumed to be constant). It is shown readily that when $D_a = D_b = D$, $b = 1 - a$ is a general solution to eqs 3 and 4 with the boundary conditions above. For simplicity, we replace the solution of a and $1 - b$ by the function u. Equations 3 and 4 may then be reduced to the following dimensionless form

$$\frac{\partial u}{\partial \tau} = \left(\frac{\partial^2}{\partial z^2} + \frac{\partial^2}{\partial r^2} + \frac{1}{r}\frac{\partial}{\partial r}\right)u \tag{5}$$

with the boundary conditions

electrode	$z = 0$	$r_b \leq r \leq r_0$	$\frac{\partial u}{\partial z} = -(k_f' + k_b')u_0 + k_b'$
block	$z = 0$	$0 \leq r < r_b$	$\frac{\partial u}{\partial z} = 0$
axis of symmetry	$0 < z < \infty$	$r = 0$	$\frac{\partial u}{\partial r} = 0$
cylinder edge	$0 < z < \infty$	$r = R_0$	$\frac{\partial u}{\partial r} = 0$
diffusion layer	$z \to \infty$	$0 \leq r \leq r_0$	$\frac{\partial u}{\partial z} = 0$

where u_0 is the value of u at $z = 0$, and where the coordinates r and z have been nondimensionalised with respect to the parameter R_0 ($r = R/R_0$, $z = Z/R_0$) and time according to

$$\tau = \frac{Dt}{R_0^2} \tag{6}$$

and the rate constants have been nondimensionalised according to $k_b' = k_b R_0/D$ and $k_f' = k_f R_0/D$. The introduction of the dimensionless time variable, τ, results in a transformed characteristic time scale, t_c. As a consequence, the scan rate, ν, is also transformed to its dimensionless form, ν_{dl}. We define the experimental time scale, t_c, as

$$t_c = \frac{2(E_f - E_i)}{\nu} = \tau_c\frac{R_0^2}{D} \tag{7}$$

where E_i and E_f are respectively the initial and final potentials

of the forward part of the voltage sweep. The dimensionless time scale is

$$\tau_c = \frac{2DRT}{nFR_0^2}\frac{(\xi_f - \xi_i)}{\nu} = 2\frac{(\xi_f - \xi_i)}{\nu_{dl}} \qquad (8)$$

where

$$\xi_x = \frac{nFE_x}{RT}; \quad x = i \text{ or } f \qquad (9)$$

and the scan rate conversion becomes

$$\nu_{dl} = \frac{nFR_0^2}{DRT}\nu \qquad (10)$$

2.2. Meshing and Discretisation. We solve eq 5 using a fully implicit finite difference method as detailed in previous publications.[23,24] The infinite Z axis boundary condition is replaced by a semi-infinite distance boundary condition according to the characteristic time scale of the cyclic voltammogram, such that $Z_{max} = 6\sqrt{(Dt_c)}$ or $z_{max} = 6\sqrt{\tau_c}$ [see ref 25, p 792]. Discretisation is performed on a square mesh where the node spacings expand geometrically away from the boundary singularity between the electrode surface and the blocked surface. This method is similar to the "expanding mesh" technique reported by Gavaghan[26] for solving microdisk problems, but with modifications to accommodate the finite cylindrical geometry and position of the boundary at $r = r_b$. We begin by meshing the solution region at points (r_i, z_j) where $i = 0, 1, 2,..., n$ and $j = 0, 1, 2,..., m$. The mesh spacings h_i and k_j are defined as

$$h_i = r_{i+1} - r_i \qquad \text{for } i = 0, 1,..., n-1$$
$$k_j = k_{j+1} - k_j \qquad \text{for } j = 0, 1,..., m-1$$

where $r_0 = 0$, $z_0 = 0$, $r_n = 1$, and $z_m = z_{max}$. We seek an approximate solution vector, **u**, to the exact concentration solution $u(r_i, z_j)$ at each point on the mesh. The element in the vector **u** for a species at a location $u(r_i, z_j)$ is denoted $U_{i,j}$. Our chosen method requires the mesh to expand geometrically away from the electrode-block boundary $(r = r_b)$. Three new parameters are introduced to describe the mesh: the expansion factor, f, the initial mesh spacing, h_{last}, and the number of nodes spanning the block surface, n_b. The expanding mesh is now described as:

$$h_{n_b-1} = h_{n_b} = h_{last}$$
$$h_{n_b-i} = fh_{n_b-i+1} \qquad \text{for } i = 2, 3, ..., n_b$$
$$h_{n_b+i} = fh_{n_b+i-1} \qquad \text{for } i = 1, 2, ..., (n_b - 1)$$
$$k_0 = h_{last}$$
$$k_{j+1} = fk_j \qquad \text{for } j = 0, 1, ..., (n_b\text{-}1)$$

To accommodate the finite solution space, we truncate the last node spacings at the limits of the grid: $h_0 = r_1$, $h_n = 1 - r_n$, $k_n = z_{max} - z_n$.

Any mesh with specified values of z_{max} may be fully characterized by the expansion factor, f, and the initial mesh separation at the annulus, h_{last}. An example mesh with $f = 1.25$ and $h_{last} = 10^{-2}$ is shown in Figure 2.

2.3. Finite Difference Formulation. The finite difference formulation of the differential operators is derived from Taylor
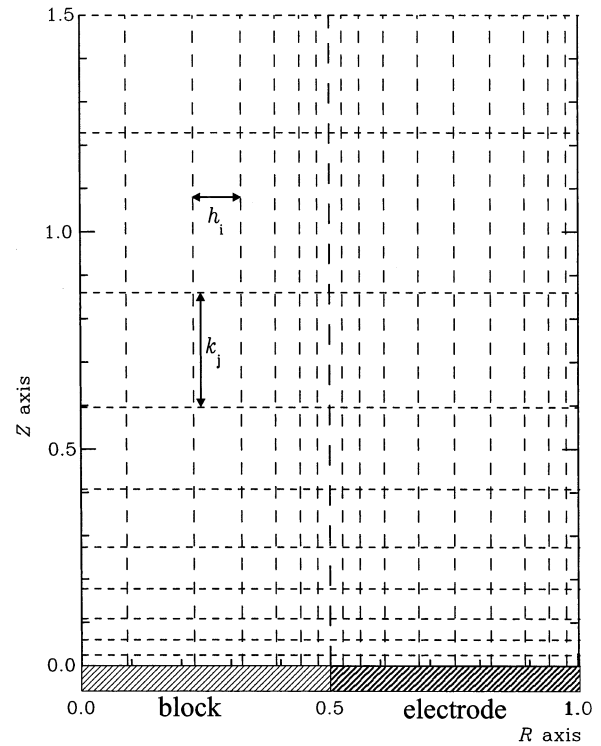
Figure 2. Example discretisation mesh with $f = 1.25$, $h_{last} = 10^{-2}$, and $r_b = 0.5$ ($\theta = 0.25$).

expansions (see appendix of ref 26)

$$u_{rr} \approx \frac{2(h_{i-1}U_{i+1,j} - (h_{i+1} + h_i)U_{i,j} + h_iU_{i-1,j})}{h_{i-1}h_i(h_i + h_{i-1})}$$

$$u_r \approx \frac{(h_{i-1}^2U_{i+1,j} - (h_{i-1}^2 - h_i^2)U_{i,j} - h_i^2U_{i-1,j})}{h_{i-1}h_i(h_i + h_{i-1})}$$

$$u_{zz} \approx \frac{2(k_{j-1}U_{i,j+1} - (k_{j+1} + k_j)U_{i,j} + k_jU_{i,j-1})}{k_{j-1}k_j(k_j + k_{j-1})}$$

2.4. Implementing the Boundary Conditions. At the cylindrically symmetric z axis, we make use of the MacLaurin expansion for u_r at $r = 0$

$$\frac{1}{r}u_r = u_{rr}$$

We impose Neumann boundary conditions by assigning fictitious concentration values outside the domain. For the axis of symmetry $(r = 0)$, $U_{-1,j} = U_{1,j}$ and $h_{-1} = h_0$, whereas at $r = 1$, $U_{i-1,j} = U_{i+1,j}$ and $h_{n+1} = h_n$. At the insulating surround, we use a one-sided second-order Taylor expansion

$$\frac{\partial u_i}{\partial z} \approx -\left(\frac{k_0^2U_{i,2} - (k_0 + k_1)^2U_{i,1} + k_1(k_1 + 2k_0)U_{i,0}}{k_0k_1(k_1 + k_0)}\right) \qquad (11)$$

to implement the boundary conditions at the electrode and block surface, such that

$$U_{i,0} = \frac{\phi(k_0 + k_1)^2U_{i,1} - \phi k_0^2U_{i,2}}{\phi(k_1 + 2k_0)} \qquad (12)$$

Study of Partially Blocked Electrodes. Part 1

J. Phys. Chem. B, Vol. 107, No. 7, 2003 **1619**

for $i = 0, 1, ..., (n_b - 1)$, and

$$U_{i,0} = \frac{\phi(k_0 + k_1)^2 U_{i,1} - \phi k_0^2 U_{i,2} + k_b'}{k_f' + k_b' + \phi(k_1 + 2k_0)} \quad (13)$$

for $i = n_b, (n_b + 1), ..., n$ where $\phi = 1/k_1 k_0 (k_1 + k_0)$.

Note that the electrode surface boundary condition is implemented arbitrarily at the node $i = n_b, j = 0$. A block boundary condition could equally have been used, but if h_{last} is sufficiently small, negligible effect on the current may be assumed. The current may therefore be evaluated across only the electrode surface from $r = r_b$ to $r = 1$, and may be calculated in dimensionless form as

$$\psi = \frac{1}{\sqrt{\nu_{dl}}} \int_{r_b}^{1} \left(\frac{\partial a}{\partial z}\right)_{z=0} r \, dr \quad (14)$$

The total electrode current, I, is the sum of all currents at N_{block} units

$$I = \pi R_0 F D [A]_{bulk} N_{block} \sqrt{\nu_{dl}} \psi \quad (15)$$

Insertion of eq 10 and the relationship $N_{block} = A_{elec}/\pi R_0^2$ yields

$$I = [A]_{bulk} A_{elec} \sqrt{\frac{F^3 D \nu}{RT}} \psi \quad (16)$$

in which F is the Faraday constant, $[A]_{bulk}$ is the bulk concentration of species A, R is the molar gas constant, and the number of electrons transferred at the electrode surface, n, is equal to one. It should be noted that the value of ψ yields a direct measurement of the current per unit area at the electrode surface and is the analogue of the *attenuation factor* used in steady-state rotating disk experiments in previous work.[9−12,27] The similarity between eq 16 and the linear sweep voltammetric current equation for linear diffusion should be noted; in the limit of θ tending to zero, the dimensionless peak current ψ_{max} should equal 0.4463 for an electrochemically reversible reaction. Equation 14 is evaluated using the following simple quadrature scheme (Simpson's rule)

$$\psi = \frac{1}{\sqrt{\nu_{dl}}} \sum_{i=n_b}^{n-1} \left(r_i \frac{\partial u_i}{\partial z} + r_{i+1} \frac{\partial u_{i+1}}{\partial z}\right)(r_i + r_{i+1}) \quad (17)$$

where the flux is measured using eq 11. To model the transient behavior, we employ a multiple level FIRM algorithm as detailed by Feldberg.[28,29] At any particular time step, t, the vector solution for that iterate may be found by solving the vector equation

$$\mathbf{q}^t = \mathbf{M}^t \mathbf{u}^t \quad (18)$$

for $\mathbf{u}^t$, where $\mathbf{u}^t$ is a vector of unknown concentrations of length $2(n + 1)(m - 1)$, $\mathbf{M}^t$ is a sparse matrix of size $2(n + 1)(m - 1) \times 2(n + 1)(m - 1)$ and $\mathbf{q}^t$ is a known vector of length $2(n + 1)(m - 1)$. The starting vector $\mathbf{q}^0 = 1$ is used along with the FIRM simple start-up protocol described in ref 28.

2.5. Simulation Results. We investigate the transient behavior of the blocked surface assuming species A is inert at the electrode blocking material surface. Computational restrictions make thorough investigations of the high θ case considerably more difficult because of the limited space over which the current will be evaluated compared to the total simulation space necessary. We therefore restrict ourselves to the arbitrary limits

of $\theta = 0.1$ and 0.9, within which to simulate. For the case where $\theta = 0$, linear-diffusion results are employed, to validate the limits of the two-dimensional simulations. In all cases, we will simulate between the kinetic limits of reversible and irreversible electrode kinetics. To characterize the transient behavior of the partially blocked electrode, cyclic voltammetry is employed in all analysis. We analyze the maximum dimensionless peak height, ψ_{max}, and also the peak-to-peak separation, $\Delta \xi_p$.

Amatore[16] has used approximate analytical theory to characterize the theoretical and experimental behavior of the PBE (where the electrode has microdisk geometry) under cyclic voltammetric conditions using a one-dimensional model. The model assumes that electrode surface blocking effects are of microscopic size, and therefore, nonlinear diffusion is confined to a layer of thickness μ, adjacent to the electrode surface, which is thin compared to the total diffusion layer. Nonlinear diffusion occurs under stationary conditions in this layer, and therefore, the flux from the bulk solution into the layer is equal to that to the electrode surface. The primary result is that the response of a blocked electrode is the same as a bare electrode of the same surface area but with an apparent rate constant[16] of $k_{dl}^0(1 - \theta)$.

This paper quantitatively addresses the issue of how the electrode response changes with scan rate and coverage where the block assumes disk geometry. In the following simulations, θ is varied between the starting and finishing values of 0.1 and 0.9, respectively, with increments of 0.1. Dimensionless scan rates were chosen to cover a large range of experimental conditions. An upper estimate of $\nu_{dl} = 10 \times F/RT$ was chosen because beyond this point it is reasonable to expect linear diffusion to dominate the characteristic current. Simulations were therefore run by varying the three parameters ν_{dl}, θ, and k_{dl}^0 accordingly, with $\alpha = \frac{1}{2}$. Three-dimensional hyper-surfaces using arrays containing $7 \times 9 \times 6$ variants were generated for the characteristic cyclic voltammetric parameters ψ_{max}, and $\Delta \xi_p$. Although it may be possible to use multidimensional interpolation and optimization algorithms, by using simple trends in the hyper-surfaces, we reduce the complexity of the data, enabling a greater insight into the CV response.

2.6. Analysis. *2.6.1. Analytical Limit.* We solve the quasi-reversible couple with equal diffusion coefficients (D) using an integral-equation method as detailed in the Appendix. Results for ψ_{max} and $\Delta \xi_p$ were generated for various values of the parameter Λ, which relates to the simulation parameter as $\Lambda = \log k_{dl}^0/\nu_{dl}$. Ordinarily,[30] $\alpha = \frac{1}{2}$, and it is this case that is considered here.

2.6.2. Peak Current. Figure 3, parts a−f, details the variation of current with $k_{dl}^0(1 - \theta)$ for fixed values of ν_{dl} and θ. As can be seen at low scan rates, the constant θ curves show little variation with ν_{dl} and tend to a single function of the parameter $k_{dl}^0(1 - \theta)$, in agreement with the theory presented by Amatore.[16] At higher scan rates, however, significant variations in the dimensionless current with θ are observed, the result of comparably sized diffusion layer length and electrode block size. In all cases, the variation of ψ_{max} for all ν_{dl} and θ appears to follow approximately a "Fermi−Dirac" type function, allowing any data set at constant θ to be reduced to a set of four parameters (ψ_{max}^0, ψ_{max}^∞, γ, and δ) defined by the function

$$\bar{\psi}_{max} = \frac{\psi_{max} - \psi_{max}^0}{\psi_{max}^\infty - \psi_{max}^0} = \frac{e^{\delta \log_{10}(k \circ (1-\theta)) + \gamma}}{1 + e^{\delta \log_{10}(k \circ (1-\theta)) + \gamma}} \quad (19)$$

where ψ_{max}^∞ and ψ_{max}^0 are the limits of ψ_{max} as k_{dl}^0 tends to infinity and zero, respectively. It is assumed that the data are
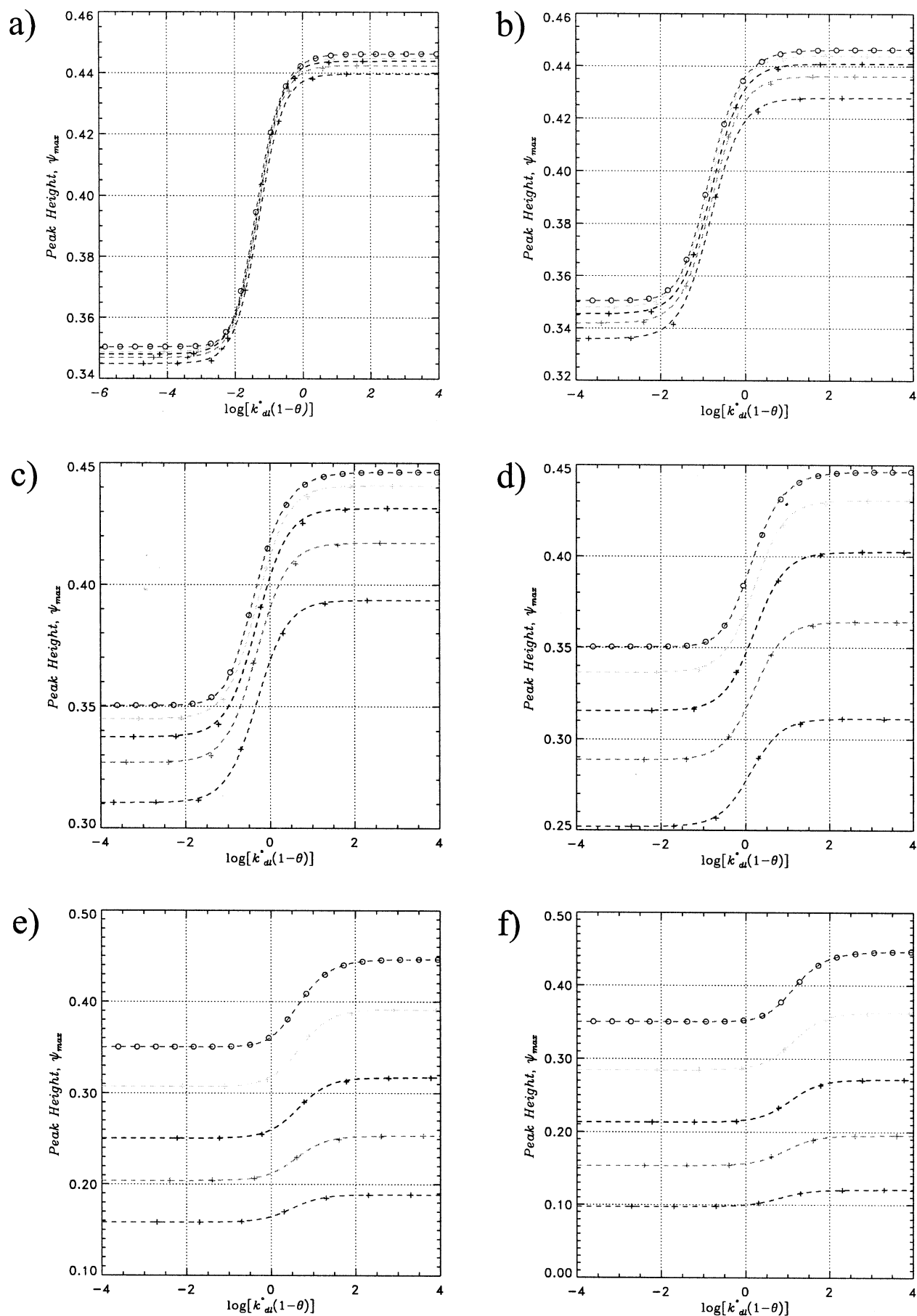
Figure 3. Peak current (ψ_{max}) responses at PBE with ν_{dl} = (a) 3.89×10^{-3}, (b) 3.89×10^{-2}, (c) 3.89×10^{-1}, (d) 3.89×10^{0}, (e) 3.89×10^{1}, and (f) 3.89×10^{2}. Simulated points (+) and fitted function (- -) are shown for θ values of (top to bottom) 0.2, 0.4, 0.6, and 0.8. Analytical results for reversible linear-diffusion (eq 21) are overlaid (○).

Study of Partially Blocked Electrodes. Part 1

J. Phys. Chem. B, Vol. 107, No. 7, 2003 **1621**

sufficiently complete to allow the determination of the limits ψ_{max}^∞ and ψ_{max}^0. The parameters δ and γ are functions of both ν_{dl} and θ, which, should they be sufficiently smooth, may be approximated using a polynomial surface fit or else calculated by an interpolation technique. Least squares curve fitting of the $\tilde{\psi}_{max}$ data was performed and the appropriate working surfaces in (ψ_{max}^0, ψ_{max}^∞, γ, and δ) determined (see Appendix).

2.6.3. Peak Separation. The peak separation shows a much less complex dependence on the variable $k_{dl}^0(1 - \theta)$ than the maximum peak current. In fact at scan rates less than $\nu_{dl} = 10^{-3}$, it is difficult to differentiate surfaces of the θ range studied. Moreover, the data presented in Figure 4, parts a–c, illustrate that, at high scan rates when deviation does occur, it may only be observed in the reversible and quasireversible domains. In Figure 4, the data from cyclic voltammetry with pure linear diffusion are overlaid. These data agree well with results from the semi-integral method; however, it is noticeable that there is a minor discrepancy between the two data sets as θ tends to zero. This may be attributed to time-stepping discretisation errors, brought about by having insufficient points to accurately approximate the derivative $\partial u/\partial \tau$ (initial simulations were run[31] with 2.5 mV separating successive iterates). When test simulations were run with sufficiently small time steps, the peak separation converged (in the $\theta = 0$ limit) to the theoretical value of 59 mV. Because the peak separation data were sufficiently close to the theoretical linear diffusion result for all but the most extreme cases of θ, the subsequent data were modeled using the function given in the Appendix.

2.7. Results for an Isolated Diffusion Domain. Two simple extremes are considered. In the first, the current to a circular electrode surface of radial size, $R_0 = 20$ μm with, at its center, a block of radius varying between $R_b = 0$ and $R_b = R_0$. In the second, the current is calculated for a block of radius $R_b = 20$ μm with a surrounding electrode between radius sizes of $R_0 = R_b$ and $R_0 = 5R_b$. In both cases, the experimental scan rate was held at 0.5 V s^{-1}, and homogeneous rate constants were 0.001, 0.025, and 1 cm s^{-1}. The current trends are illustrated in Figure 5, parts a and b. In Figure 5b, we observe a rapid increase from zero current between $R_0 = 20$ μm and $R_0 = 21$ μm where the largest change in θ occurs, followed by a slower increase dominated by the R_0 dependence of the current. For reversible electrode kinetics, the current tends to the linear-diffusion limit. In the case of Figure 5a, the current varies between the linear-diffusion limit (between reversible and irreversible limits) and decreases to zero as the block fills the base area of the diffusion domain.

2.8. Extension to Macroscopic Systems of Cubic and Hexagonal Geometry. Figure 6, parts a and b, shows cubic and hexagonal arrangements of disks of an arbitrary radius. The periodicity, p, of the arrangements is the nearest-neighbor center-to-center separation. Overlaid on the two diagrams are squares/rectangles which enclose the area associated with each block, A_{block}. The microscopic coverage, θ, is given by $\pi R_b^2/A_{block}$ and the global coverage, Θ, is given by $(N_{block}\pi R_b^2/N_{block}A_{block}) = \theta$. Therefore, by considering just one diffusion domain, we will be considering the whole of the electrode; that is, the ψ_{max} and $\Delta\xi_p$ values for this domain will be equal to that for the whole electrode.

Unfortunately, our domains (squares/rectangles) do not correspond to those for which we have simulated data (circles). We thus approximate each square/rectangle as a circle of area A_{block} with radius R_0. This is a simple task for the cubic arrays for which we have $p^2 = \pi R_0^2$. The hexagonal arrangement is slightly more complicated; from Figure 6b, we can infer $x = p$
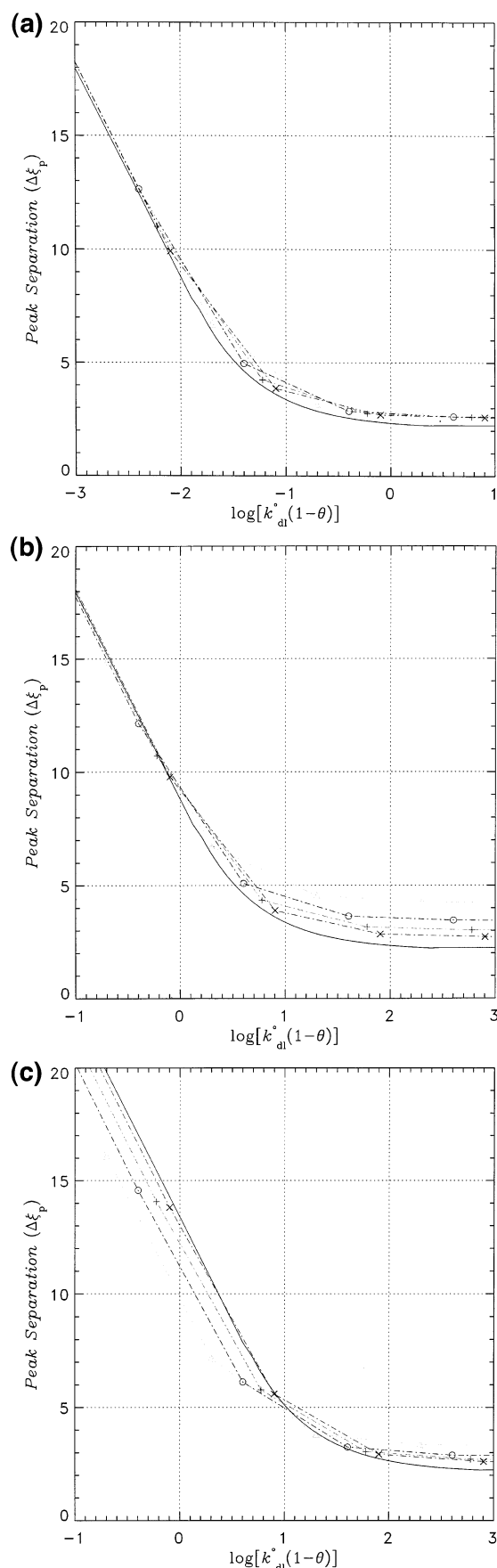
Figure 4. Peak separation ($\Delta\xi_p$) responses for the blocked electrode with $\nu_{dl} =$ (a) 3.89×10^{-3}, (b) 3.89×10^1, and (c) 3.89×10^2. Simulated points and fitted function are shown for θ values of (top to bottom) 0.2 ($\times$), 0.4 (+), 0.6 ($\bigcirc$), and 0.8 ($\triangle$). Analytical results for reversible linear diffusion (eq 21) are overlaid (—).

(a)

(b)
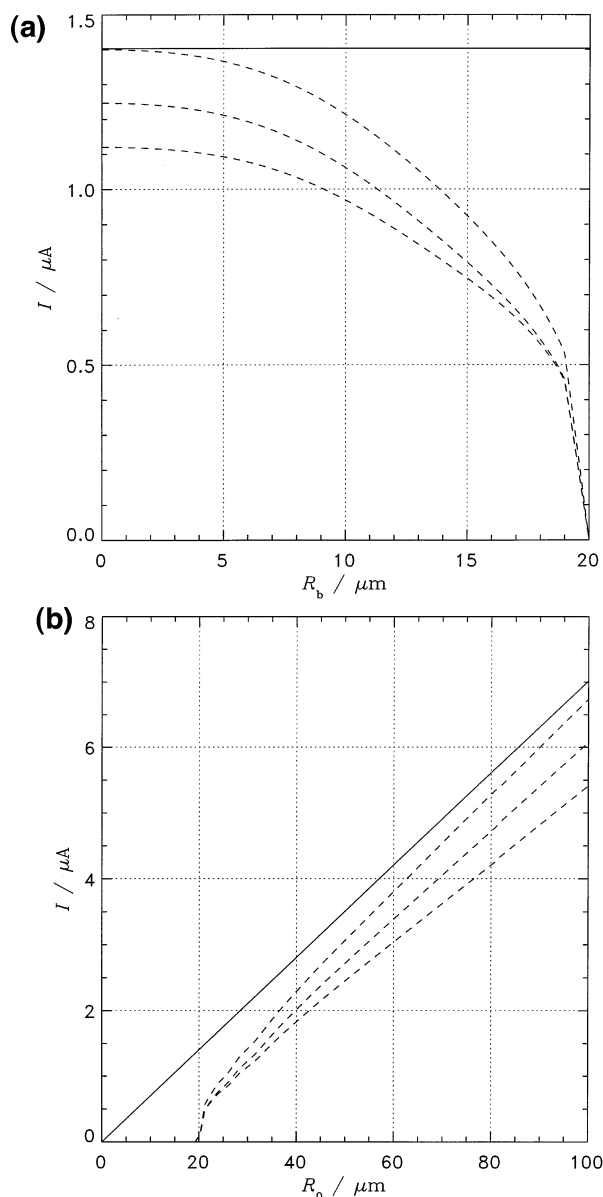
Figure 5. Theoretical current response for blocks on an isolated circular electrode surface with (bottom to top) $k^\circ = 10^{-3}$, 2.5×10^{-2} and 1 cm s^{-1}. (a) Electrode radius, R_0, is fixed at 20 mm. (b) Block radius, R_b, is fixed at 20 μm. Reversible linear-diffusion current for unblocked electrode surface is overlaid (—).

and $y = \sqrt{3}/2p$. Therefore, $A_{block} = \sqrt{3}/2p^2 = \pi R_0^2$. Ideally, if the domain around each block was circular instead of a square/rectangle, R_0 would be $0.5p$. Hence, the hexagonal array ($R_0 = 0.525p$) fits the approximation better than the cubic arrangement ($R_0 = 0.564p$), and we anticipate better agreement between the theory and experiment with the hexagonal electrodes.

3. Experimental Section

3.1. Chemical Reagents. Electrolyte reagents, *N,N,N′,N′*-tetramethyl-*para*-phenylenediamine (TMPD, Aldrich Chemical Co.) and tetrabutylammonium perchlorate (TBAP, Fluka, electrochemical grade) were purchased in the purest commercially available grade. Acetonitrile used to make the electrolyte solutions was purchased from Fisons (dried and distilled). All solutions were outgassed with oxygen-free nitrogen (BOC Gases, Guildford, Surrey, U.K.) for at least 15 min prior to experimentation. All experiments were conducted at 20 ± 2 °C.
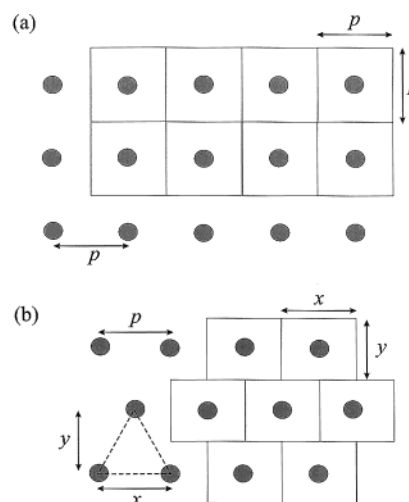
Figure 6. (a) Cubic packing arrangement. (b) Hexagonal packing arrangement.

3.2. Instrumentation. Electrochemical experiments were conducted in a conventional three-electrode cell, employing a 4.85×4.85 mm square partially blocked gold film working electrodes (vide infra), a gold wire counter electrode and a silver wire quasireference electrode. For experiments at a nonblocked electrode surface, a 3 mm diameter gold rod was sealed in Teflon, and used as the working electrode. This electrode was polished using a 1.0 μm alumina slurry (Beuhler, Lake Bluff, Il, USA) and rinsed in water and acetonitrile prior to deployment. Electrochemical data were recorded using a commercially available computer-controlled potentiostat (AUTOLAB PG-STAT30, Eco-Chemie, Utrecht, The Netherlands).

The partially blocked gold film electrodes were prepared by the following method. Glass wafers were cleaned using decon 90 (Decon Laboratories, Ltd., Hove, East Sussex, U.K.) and water prior to rinsing and sonicating in absolute ethanol. The wafers were blown dry using nitrogen. All electrodes were fabricated using standard lithographic techniques:[32] a computer generated mask was employed to produce a negative photoresist image of the blocked electrodes on the glass substrate, the latter being placed in a metal evaporator (Emitech K975). A thin film of chrome was deposited (with thickness ca. 50 nm) through the mask, followed by a coating of gold (of thickness ca. 150 nm) under the same vacuum cycle, the chrome undercoating being used to create a good adhesion layer between the glass and the gold. Ten electrodes, each corresponding to a known fractional coverage (0.05, 0.18, 0.25, 0.35, and 0.5), were fabricated with either cubically or hexagonally arranged insulating block geometry. In the former case, the electrochemically inactive disks had radii of 25.23, 47.70, 56.42, 66.76, or 79.79 μm, all separated (center-to-center) with a periodicity of 200 μm, resulting in factional coverage values of 0.05, 0.18, 0.25, 0.35, and 0.5. For the hexagonal blocking geometry, the insulating disks were again separated (center-to-center) with a periodicity of 200 μm and had radii of 23.48, 44.39, 52.50, 62.21, or 74.25 μm to yield the corresponding surface coverage indicated above. In both cases the center-to-center separation is relatively large compared to usual Nernst layer thicknesses, so that the total coupling between the diffusion layers observable at low scan rates may be prevented. The electrodes were gently cleaned with acetonitrile and dried in air immediately prior to use. Electrical connection to the PBE was ensured by lithographically producing a gold-film connecting lead on the glass substrate. A piece of copper tape (with conductive adhesive underside) was placed at the top of the lead, so as to enable

Study of Partially Blocked Electrodes. Part 1

J. Phys. Chem. B, Vol. 107, No. 7, 2003 **1623**

electrical connection to the glass-based electrode. For electrochemical experiments, performed by the oxidation of ca. 1 mM TMPD in 0.1 M TBAP in acetonitrile, the exposed gold-film connector was covered up using a cosmetic depilatory wax (Wax-A-Way, London), known to be insoluble in acetonitrile, and the whole electrode assembly was subsequently immersed into the electrochemical cell with the aid of a M3301R manual micromanipulator (World Precision Instruments, Stevenage, Herts., U.K.). The potential of the gold-film partially blocked electrode was scanned from −0.5 V vs Ag to no further than 0.36 V vs Ag. After experiments, the electrode was cleaned in acetonitrile.

Imaging of the partially blocked electrode produced in the method outlined above was undertaken in two ways. In the first, the undersides of the electrodes were viewed via a computer-controlled flat-bed scanner operating using a high-resolution mode. Detailed viewing via scanning electron microscopy (SEM), was achieved using a Cambridge Stereoscan scanning electron microscope.

4. Experimental Results and Discussion

4.1. Visual Assessment of the Partially-Blocked Gold Film Electrodes. Figure 7 presents images of all of the 4.85 × 4.85 mm square partially blocked electrodes employed in this work. In Figure 7a, SEM images of the cubically arranged blocking system are shown; those exhibited in Figure 7b correspond to digital images of the hexagonally packed partially blocked electrodes.

Although the resolution of the figures depicted in Figure 7b is not as great as those in Figure 7a, it can be seen that the majority of electrodes are well fabricated, and fit the "idealized" geometries drawn in Figure 6. The cubically arranged electrodes can be seen to be more "faulty" than the hexagonally packed case, with defects arising from (i) missing blocking disks, (ii) irregular geometry (see Figure 7a(i)), or (iii) electroinactive blocking disks with a nonuniform size (see Figure 7a(iv)). Although these faults are minor, and with low occurrence, they should nevertheless not be forgotten!

4.2 Experiment vs Theory. First, cyclic voltammetry experiments were performed ($0.02 \leq v/V\ s^{-1} \leq 2$) using the 3 mm diameter unblocked gold disk electrode, to determine the diffusion coefficient and heterogeneous rate constant for TMPD oxidation at a gold electrode in acetonitrile solution. Analysis of the peak current using the Randles−Sevčik equation and the peak-to-peak separation data using Nicholson's treatment[33] yielded a value of $k^0 = 1.4 \pm 0.2 \times 10^{-2}$ cm s^{-1} and diffusion coefficient (in acetonitrile) of $2.1 \pm 0.1 \times 10^{-5}$ cm^2 s^{-1}. Cyclic voltammetry was then undertaken on all of the fabricated electrodes using six scan rates of within the range $0.02 \leq v/V$ s$^{-1} \leq 1.0$. Simulations were performed to determine the theoretical response of a single diffusion domain with a radial size, R_0, of $0.564p$, in the case of the cubic electrodes, or $0.525p$, in the case of the hexagonal electrodes, where $p = 200\ \mu$m (see section 3). The value of ψ_{max} was calculated for a range of R_b values between 0 and R_0 (corresponding to $0 \leq \theta \leq 1$). Figure 8, parts a and b, shows the results of such simulations with the experimentally observed results overlaid (horizontal lines in Figure 8). The line labeled "error" is given by the equation

$$\text{error}(R_b) \propto \sum_{i=1}^{6}(\psi_{max}^i(R_b) - \psi_{max}^i(\exp))^2 \qquad (20)$$

where $\psi_{max}^i(R_b)$ is the value of ψ_{max} at the block radius R_b for
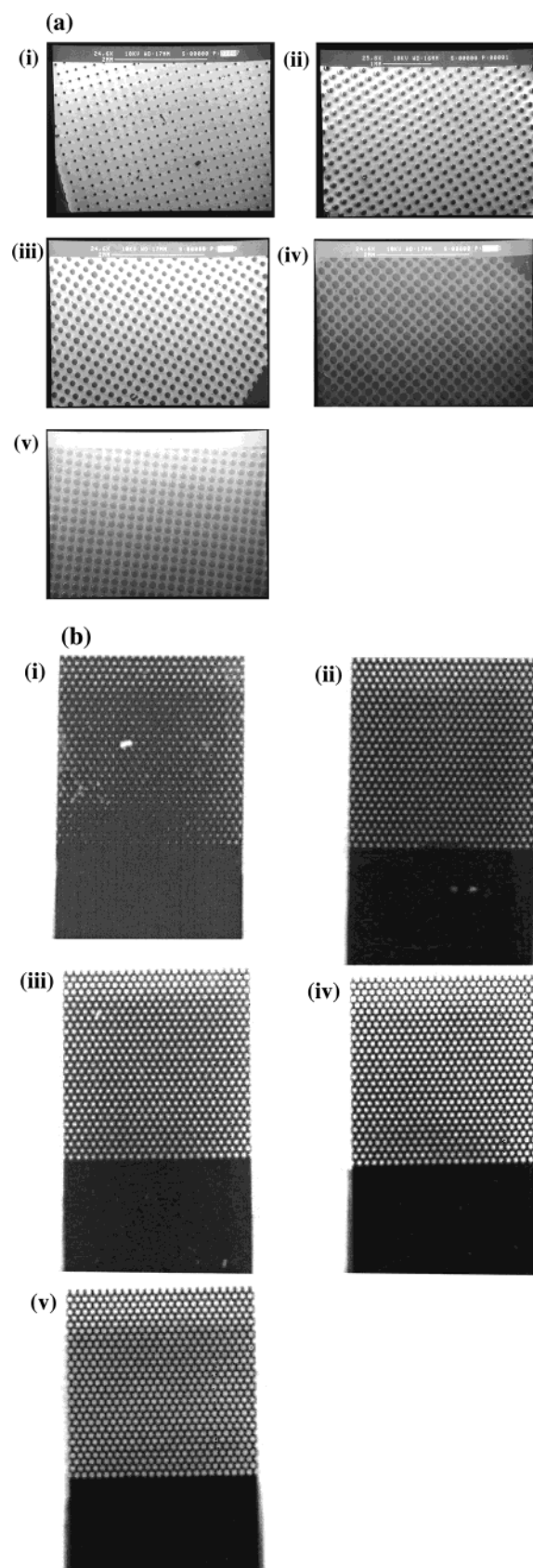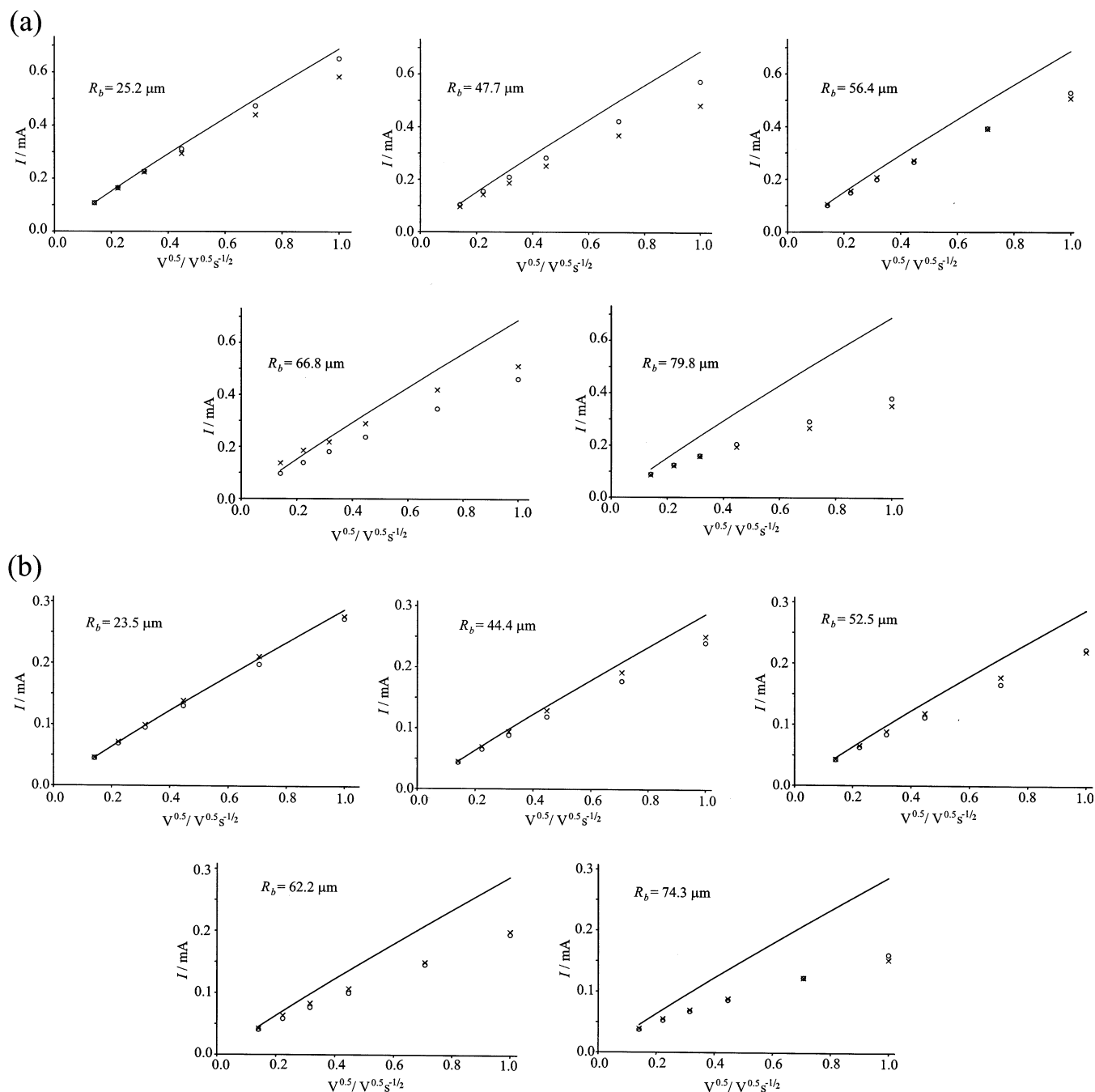

Figure 7. (a) SEM images of cubically packed and partially blocked electrodes where R_b = (i) 25.5, (ii) 47.7, (iii) 56.4, (iv) 66.8, and (v) 79.8 μm. The blocks appear as black/dark circles, whereas the light areas are the gold film. (b) Digital images of hexagonally packed partially blocked electrodes where R_b = (i) 23.5, (ii) 44.4, (iii) 52.5, (iv) 62.2, and (v) 74.3 μm. The dark areas are gold, and the white circles are the inert blocks. On both sets of electrodes, the periodicity, p, is equal to 200 μm.
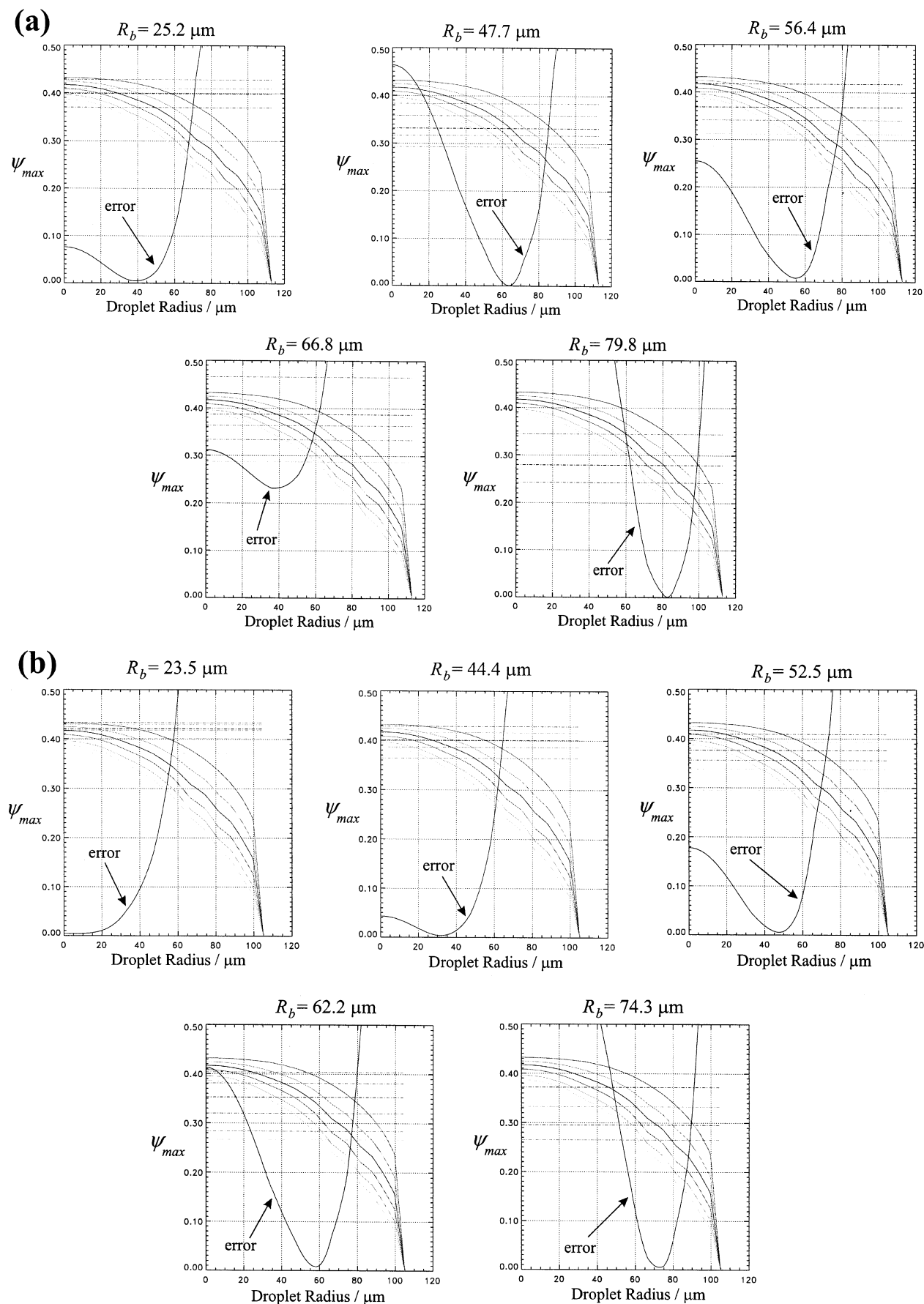
Figure 8. Simulations of the variation in the theoretically predicted value of ψ_{max} with block radius, R_b, for scan rates of (top to bottom) 0.02, 0.05, 0.1, 0.2, 0.5, and 1.0 V s^{-1}. The experimentally observed nondimensionalised currents are overlaid (- -). (a) Cubically packed electrodes where R_b = (i) 25,5, (ii) 47.7, (iii) 56.4, (iv) 66.8, and (v) 79.8 μm and R_0 = 112.8 μm. (b) Hexagonally packed electrodes where R_b = (i) 23.5, (ii) 44.4, (iii) 52.5, (iv) 62.2, and (v) 74.3 μm and R_0 = 105.0 μm.

Study of Partially Blocked Electrodes. Part 1

J. Phys. Chem. B, Vol. 107, No. 7, 2003 **1625**

Figure 9. Plots of theoretically predicted current (○), experimentally observed current (×) and unblocked/theoretical maximum current (obtained using eq 21; —) vs the square root of the scan rate. (a) Cubically packed electrodes where R_b = (i) 25.5, (ii) 47.7, (iii) 56.4, (iv) 66.8, and (v) 79.8 μm and R_0 = 112.8 μm. (b) Hexagonally packed electrodes where R_b = (i) 23.5, (ii) 44.4, (iii) 52.5, (iv) 62.2, and (v) 74.3 μm and R_0 = 105.0 μm.

a scan rate i, ψ_{max}^i(exp) is the experimental value of ψ_{max} at the scan rate i, and i = 1, 2, 3, 4, 5, and 6 represents the six scan rates ν = 0.02, 0.05, 0.1, 0.2, 0.5, and 1.0 V s^{-1} respectively. The predicted block radius is thus the value of R_b for which the error is a minimum. Table 1 displays the "actual" and theoretically predicted block radii, R_b, for the two sets of fabricated electrodes (cubic and hexagonal geometries). Figure 9, parts a and b, illustrates the variance of the experimental, predicted, and unblocked current with the square root of the scan rate, in which the value of R_b used in the calculation for the predicted current is the "actual" R_b value shown in Table 1.

Comparing the data in Table 1, we see that the model works best for electrodes of a high coverage (high R_b value). The simulations in Figure 8, parts a and b, highlight a reason for this; it is not until we exceed ca. R_b = 20 μm that there is a

TABLE 1: Predicted and Actual Radii of Blocks/Inert Disks on the Fabricated Electrode Surfaces

cubic packed (R_0 = 112.8 μm)		hexagonal packed (R_0 = 105.0 μm)	
actual R_b/ μm	predicted R_b/ μm	actual R_b/ μm	predicted R_b/ μm
25.5	40	23.5	0−20
47.7	63	44.4	33
56.4	55	52.5	48
66.8	38	62.2	58
79.8	83	74.3	73

noticeable decline in the dimensionless peak current, ψ_{max}. Indeed, for low scan rates, the current does not change until R_b ∼ 40 μm. Thus, for *small* values of R_b, the simulated current curve is approximately independent of R_b. This is evident for

the hexagonal electrode where $R_b = 23.5 \mu m$ (Figure 8b(i)) where we do not observe a minimum. Ideally, for electrodes with low coverage, we should only use high scan rate experimental data to predict R_b values because minima in the error function (eq 20) are more pronounced for high scan rates. The data for the hexagonal electrodes in Table 1 are very promising; at high coverage, the theory is almost in complete agreement with the experimental results. As anticipated in section 2.8, the experimental results for the hexagonal electrodes fit the theory better than those for the cubically arranged electrodes. However, this might not be entirely due to the $0.5p$ factor. As mentioned in section 4.1, the fabricated electrodes are not perfectly formed, and in general, the standard of the hexagonal electrodes is better than the cubic ones. Indeed, the three disappointing results in Table 1, in which theory and experiment are not within 30% (cubic: $R_b = 25.5$, 47.7, and 66.8 μm), occur for electrodes with the most significant defects (see Figure 6). Figure 9, parts a and b, illustrates this point succinctly. The agreement of the experimental data with the theory suggests that the approximation made in section 2.8, where we equated the squares/rectangles to circles of radius R_0, appears to be viable.

In summary, the data obtained at hexagonally packed insulating disks appear to be in better agreement with the theory than that arising from a cubically arranged geometry. We suggest this is primarily due to the hexagonal R_0 conversion factor being closer to 0.5 than the cubic conversion factor. However, the quality of the model electrodes may play a role. Furthermore, the best agreement between theory and experiment occurs for electrodes with *high* coverage; at low coverage, only *high* scan rates should be used when attempting to determine experimentally the radius of blocking disks.

5. Conclusions

In this paper, we sought to simulate the behavior of electrodes partially covered with uniformly distributed and monodisperse disks, between the limits of reversible and irreversible electrochemistry. The validity of our approach has been illustrated via reference to experimental data observed from two different well-defined geometric ensembles of blocking disk-shaped particles. The very good agreement between theory and experiment observed for the uniformly distributed case considered here suggests that this method *may* be applied, with suitable modification, to the study of electrodes covered with a randomly dispersed blocking system. It is this case that we will consider in a subsequent paper.[21]

Appendix

A.1. Computation. To solve eq 18, the NAG library F11 (preconditioned Krylov subspace) methods[34,35] were employed. In particular, as the incomplete LU preconditioner[46] ($L_{FILL} = 0$, $D_{TOL} = 10^{-14}$) (**F11ZAF, F11BAF**) and the[37,38] BICGSTAB-

(R = 4) (**F11DCF**) were used to solve the resulting linear system of equations. The simulation code was written in C++ and run on a Silicon Graphics Origin 2000 server. All simulations were solved with $D_A = D_B$ and $E^{0'} = 0$ V, and the parameters h_{last} and f were set to the values of $10^{-5}\sqrt{\theta}$ and 1.15, respectively.[39] The former ensured that the number of mesh nodes within the blocked surface ($0 \le r \le r_b$) was constant for all simulations and ensures that the error propagated by the boundary discontinuity was consistent.

Cubic spline fitting and spline evaluation was used performed on the cyclic voltammetry data using NAG routines **E02BAF** and **E02BBF**. The fitting algorithm automatically placed ties at every second data point. Once the raw CV data had been collected, all further computation required for the PBE modeling was performed using IDL 5.0.

To ensure that ψ_{max} and $\Delta\xi_p$ could be determined from simulations in a consistent manner, the cyclic voltammetry was started at not less than -0.2 V oxidative of $E^{0'}$ and the potential at scan reversal was maintained at 0.2 V more reductive than the initial peak maximum. Failure to do so may result in inconsistent measurement of backward peak position [ref 25, Table 6.5.1].

A.2. Analytical Limit. Linear diffusion results were generated by numerically solving the integral equation

$$I(t) = \Gamma\epsilon^{-\alpha}\left(FA\sqrt{D}C_0 - \frac{1+\epsilon}{\sqrt{\pi}}\int_0^t \frac{I(u)}{\sqrt{t-u}}\,du\right) \quad (21)$$

where $\Gamma = k^0/D$, $\epsilon = \exp[nF/RT(E(t) - E^{0'})]$, $E(t) = E_i + vt$, and $\alpha = \frac{1}{2}$. This technique has been used by a number of authors previously.[33,40,41] However, in the interest of completeness, results in the desired range were recalculated. A total of 500 iterations were used in the summation of the current integral. The potential at which the voltage was reversed was sufficiently beyond the current peak that the peak separation was invariant to changes in this reversal. The peak data were analyzed using the cubic spline method (vide supra). The peak-separation data were fitted by splicing three separate functions

$$\Delta\xi_p = 2.23 \qquad \log_{10}\Lambda > 1.61$$

$$\Delta\xi_p = 2.11 + 13.46\exp[-1.743(\log_{10}\Lambda - 1.156)]$$
$$-0.64 \le \log_{10}\Lambda > 1.61$$

$$\Delta\xi_p = 1.505 - 9.178\log_{10}\Lambda \qquad \log_{10}\Lambda < -0.64$$

where

$$\Lambda = k^0/\sqrt{DFv/RT} = k_{dl}^0\sqrt{1/v_{dl}}$$

A.3. Peak Current. The process for empirically determining simple forms of the parameters required in the Fermi−Dirac fitting are described below. Values of δ showed no dependence on the parameters v_{dl} and θ, having mean value of 2.76 and standard deviation 0.12. The parameter γ showed variation in both v_{dl} and θ. Therefore, a bilinear interpolation method[42] was

TABLE 2: Dimensionless Peak Current (ψ_{max}^{∞}) Working Surface Data for Partially Blocked Electrode

$v_{dl}\backslash\theta$	0.1	0.2	0.3	0.4	0.5	0.6	0.7	0.8	09
3.89×10^{-3}	0.4452	0.4449	0.4445	0.4439	0.4433	0.4424	0.4413	0.4397	0.4368
3.89×10^{-2}	0.4449	0.4439	0.4426	0.4409	0.4388	0.4361	0.4327	0.4278	0.4197
3.89×10^{-1}	0.4438	0.4407	0.4366	0.4314	0.4251	0.4172	0.4072	0.3937	0.3723
3.89×10^{0}	0.4403	0.4305	0.4178	0.4024	0.3847	0.3642	0.3403	0.3112	0.2716
3.89×10^{1}	0.4162	0.3913	0.3587	0.3170	0.2936	0.2533	0.2298	0.1887	0.1449
3.89×10^{2}	0.3995	0.3625	0.3208	0.2715	0.2409	0.1951	0.1648	0.1206	0.0787

used to determine γ from a 3-D surface of γ against both ν_{dl} and θ.[43] The two parameters $\psi_{max}^0(\theta,\nu_{dl})$ and $\psi_{max}^\infty(\theta,\nu_{dl})$ showed significant variation in both ν_{dl} and θ. To accommodate the experimental limits outside the simulated range, the following boundary conditions were introduced:

$$\psi_{max}^0(1,\nu_{dl}) = 0 \qquad \psi_{max}^\infty(0,\nu_{dl}) = \Psi_p\left(\Lambda,\frac{1}{2}\right)$$

$$\psi_{max}^0(\theta,0) = \Psi_p\left(\Lambda,\frac{1}{2}\right) \quad \psi_{max}^\infty(\theta,0) = \Psi_p\left(\Lambda,\frac{1}{2}\right)$$

$$\psi_{max}^0(\theta,\infty) = \Psi_p\left(\Lambda,\frac{1}{2}\right)(1-\theta)$$

$$\psi_{max}^\infty(\theta,\infty) = \Psi_p\left(\Lambda,\frac{1}{2}\right)(1-\theta)$$

where $\Psi_p(\Lambda,\alpha)$ is the dimensionless peak current predicted by the linear-diffusion theory at $\Lambda = k_{dl}^0/\nu_{dl}$. A bilinear interpolation method was employed to determine ψ_{max}^0 from a 3-D surface of ψ_{max}^0 vs. ν_{dl} and θ, and ψ_{max}^∞ from a 3-D surface of ψ_{max}^∞ vs ν_{dl} and θ.[43] The surface data for ψ_{max}^∞ are presented in Table 2.

References and Notes

(1) Contamin, O.; Etman, M. *J. Electroanal. Chem.* **1982**, *136*, 259.

(2) Lindemann, J.; Landsberg, R. *J. Electroanal. Chem.* **1971**, *30*, 79.

(3) Lindemann, J.; Landsberg, R. *J. Electroanal. Chem.* **1971**, *29*, 261.

(4) Lindemann, J.; Landsberg, R. *J. Electroanal. Chem.* **1970**, *25*, 20A.

(5) Scheller, F.; Landsberg, R. *Z. Phys. Chem.* **1970**, *244*, 273.

(6) Scheller, F.; Landsberg, R.; Wolf, H. *Electrochim. Acta* **1970**, *15*, 525.

(7) Scheller, F.; Mueller, S.; Landsberg, R. *J. Electroanal. Chem.* **1969**, *20*, 375.

(8) Scheller, F.; Mueller, S.; Landsberg, R.; Spitzer, H. *J. Electroanal. Chem.* **1966**, *19*, 187.

(9) Levart, E.; Schumann, D.; Contamin, O.; Etman, M. *J. Electroanal. Chem.* **1976**, *70*, 117.

(10) Etman, M.; Levart, E.; Schumann, D. *J. Electroanal. Chem.* **1979**, *101*, 141.

(11) Etman, M.; Levart, E.; Scarbeck, G.; Schumann, D. *J. Electroanal. Chem.* **1979**, *101*, 153.

(12) Etman, M. *J. Electroanal. Chem.* **1985**, *187*, 247.

(13) Tokuda, K.; Gueshi, T.; Matsuda, H. *J. Electroanal. Chem.* **1978**, *89*, 247.

(14) Tokuda, K.; Gueshi, T.; Matsuda, H. *J. Electroanal. Chem.* **1979**, *101*, 29.

(15) Gueshi, T.; Tokuda, K., Matsuda, H. *J. Electroanal. Chem.* **1979**, *102*, 41.

(16) Amatore, C.; Savéant, J.-M.; Tessier, D. *J. Electroanal. Chem.* **1983**, *147*, 39.

(17) Reller, H.; Kirowa-Eisner, E.; Gileadi, E. *J. Electroanal. Chem.* **1988**, *240*, 247.

(18) Shoup, D.; Szabo, A. *J. Electroanal. Chem.* **1984**, *160*, 19.

(19) Juozénas, A.; Šidlauskas, V.; Jurevičius, D. *Chemija* **1993**, *1*, 13.

(20) Survila, A.; Stasiukaitis, P.; Povilas, V.; Kanapeckaite, S.; Uksiene, V. *Chemija* **1988**, *2*, 143.

(21) Brookes, B. A.; Davies, T. J.; Fisher, A. C.; Yunus, K.; Wilkins, S. J.; Greene, P. R.; Wadhawan, J. D.; Compton, R. G. Manuscript in preparation.

(22) In the case of an ensemble of electrodes, Reller[17] suggests that the current is largely independent of basic unit shape. However, other analytical work (see Scharifker, B. *J. Electroanal. Chem.* **1988**, *240*, 366) shows that changing from a cubic to a hexagonal distribution generates a noticeable difference in the chronoamperometric current.

(23) Welford, P. J.; Brookes, B. A.; Climent, V.; Compton, R. G. *J. Electroanal. Chem.* **2001**, *513*, 8.

(24) Brookes, B. A.; Gavaghan, D. J.; Compton, R. G. *J. Phys. Chem. B* **2002**, *106*, 4886.

(25) Bard, A. J.; Faulkner, L. R. *Electrochemical Methods: Fundamentals and Applications*, 2nd ed.; Wiley: New York, 2001.

(26) Gavaghan, D. J. *J. Electroanal. Chem.* **1998**, *456*, 1.

(27) Cooke, J. *Quart. J. Appl. Math.* **1970**, *10*, 366.

(28) Mocak, J.; Feldberg, S. W. *J. Electroanal. Chem.* **1994**, *378*, 31.

(29) Feldberg, S. W.; Goldstein, C. I. *J. Electroanal. Chem.* **1995**, *397*, 1.

(30) Reiger, P. H. *Electrochemistry*; Prentice-Hall: Englewood Cliffs, NJ, 1987; p 275.

(31) For ease, dimensionless potentials are quoted to their equivalent absolute values at 298 K.

(32) Jackel, J. P. *Microtechnology* **1996**, *36*, 707.

(33) Nicholson, R. S. *Anal. Chem.* **1965**, *37*, 1351.

(34) Alden, J. A.; Compton, R. G. *J. Phys. Chem. B* **1997**, *101*, 9606.

(35) Alden, J. A.; Compton, R. G. *J. Phys. Chem. B* **1997**, *101*, 8941.

(36) Meijerink, J.; Van der Vorst, H. *Math. Comput.* **1977**, *31*, 148.

(37) Van der Vorst, H. *SIAM J. Sci. Stat. Comput.* **1989**, *13*, 631.

(38) Sleujpen, G. L. G.; Gokkema, D. R. *Electron Trans. Numer. Anal.* **1993**, *1*, 11.

(39) Gavaghan[26] has shown that these values of the initial mesh spacing, h_{last}, and expansion factor, f, lead to accurate results for the microdisk electrode.

(40) O'Dea, J. J.; Osteryoung, J.; Osteryoung, R. A. *J. Electroanal. Chem.* **1981**, *53*, 695.

(41) Matsuda, H.; Ayabe, Y. *Z. Elektrochem.* **1955**, *59*, 494.

(42) See, for example: Press, W. H.; Flannery, B. P.; Teukolsky, S. A.; Vetterling, W. T. *Numerical Recipes in C*; Cambridge University Press: Cambridge, 1988; p 105.

(43) Bilinear interpolation was only performed on simulated results. The determination of γ, ψ_{max}^0, and ψ_{max}^∞ for ν_{dl} and θ values outside the working surface was performed by linear interpolation using the limits defined in the appendix.